Model Development Of An Underwater Manipulator For Coordinated Arm-Vehicle Control

Kortney N. Leabourne * Stephen M. Rock †‡
Stanford University Aerospace Robotics Laboratory
Monterey Bay Aquarium Research Institute

ABSTRACT

This paper presents research on the hydrodynamic modeling of a manipulator for an autonomous underwater science vehicle. The focus is on improving the modeling accuracy of the in-line hydrodynamic coupling between a two-link manipulator and a small, free-floating vehicle in order to achieve better control for coordinated motion of the combined system. Loads predicted using existing models for underwater arms were determined to be off by as much as 25% when applied to a real, two-link arm in a test tank. In this new approach, an experimentally-determined model has been developed that takes into account 3-D flow effects that have previously not been included. The end result is a model that provides accurate predictions for the joint torques of a two-link arm in a form simple enough to be implemented in algorithms for precision planning and control. This project is part of a joint program between the Aerospace Robotics Laboratory (ARL) at Stanford University and the Monterey Bay Aquarium Research Institute (MBARI).

I. INTRODUCTION

A. Motivation

For underwater science research involving intervention tasks, manipulation is a required capability, allowing precise retrieval of objects and animals, as well as instrument deployment and servicing. Manipulation research in the Stanford/MBARI program has focused on automated manipulation for small, highly maneuverable robots such as the *OTTER* (Ocean Technology Testbed for Engineering Research) autonomous vehicle [11]. When a manipulator is used on this type of vehicle, particularly for fast motions, the hydrodynamic effects on the vehicle generated by motion of the arm are significant and affect the ability to achieve precise control. Autonomous capabilities for underwater manipulators provide precision low-level planning and control to coordinate the system's motion while the pilot interacts only at a high level, determining what specific task is to be performed. This requires a model form that can accurately predict the physical aspects of the flow around a manipulator. Specifically, this research addresses the issue of characterizing the in-line flow around a planar two degree-of-freedom (2 DOF) manipulator. A model that includes elbow joints and end effects for a two-link arm can provide insight for multiple-link arm models as well.

B. Background

There are many sources of work on both the modeling and control of underwater manipulators, including [4], [5], [10], [7], [3], [8], and [6]. Some of these studies have modeled underwater arms as consisting of cylindrical links, and thus building on existing 2-D theory of the in-line hydrodynamic forces (those in the same plane as the cylinder's motion) specific to this shape. Work done in simulation by Lévesque and Richard in [5] focused on the full nonlinear drag forces, using Hoerner's cross-flow principle for the pressure drag forces acting on a cylinder translating at an angle to the freestream. This states that the drag corresponds only to the component of velocity perpendicular to the longitudinal axis of a cylinder, and the effective drag coefficient is the same as for an infinitely long translating cylinder, a value of 1.1 [2]. This principle was applied using a strip theory approach on links divided into segments. The drag force on the i^{th} infinitesimal element of each link is determined by:

$$dF_i = \frac{1}{2}\rho C_d V_{y_i} \mid V_{y_i} \mid D l_i dl_i \tag{1}$$

where ρ is the fluid density, C_d is the constant drag coefficient, V_{y_i} is the component of the velocity perpendicular to the i^{th} element, D is the link diameter, l_i is the distance from the joint to the centroid of force on the i^{th} element, and dl_i is the longitudinal length of the element. The resulting total drag for the link can be determined by summing the forces on each element over the length of the link, with joint torques found by multiply-

*Doctoral Candidate, Department of Aeronautics and Astronautics, kortney@sun-valley.Stanford.EDU
†Associate Professor, Department of Aeronautics and Astronautics, rock@sun-valley.Stanford.EDU
‡Adjunct Research Engineer, MBARI

ing the elements' force components by the corresponding moment arms. In [10], Tarn developed a model for simulating the complete dynamics of an underwater vehicle and manipulator, including drag forces based on Lévesque's work (with one constant drag coefficient for all links) and added mass terms for the in-line forces, using an added mass coefficient of 1, the value used in potential flow theory.

McLain [7] was the first to do experimental work on a single rotating cylindrical link as part of the Stanford ARL/MBARI program. In that work, it was determined that the translational models with constant drag and added mass coefficients in previous literature were not accurate in predicting the forces and torques at the joint due to the 3-D pressure distribution around the entire link. McLain used a strip-theory approach that accounted for interaction between the link's segments and applied Sarpkaya's assumption that the drag and added mass coefficients are functions of distance traveled only, eventually reaching a steady state value, for each segment [9]. The drag forces for this model have the same form as in Equation (1), but the drag coefficient is now a function of distance traveled, C_d(s/D), where s/D is the total distance traveled, measured in number of diameters (see [7] for curve-fit form of function). Velocity variations cause pressure gradients along the length of the link; this results in 3-D flow from the hub to the tip, as well as around the tip, which acts to relieve the lower base pressure in areas near the tip and decrease the average steady state drag coefficient to a value below that predicted by Hoerner's theory since the 2-D in-line pressure integral has effectively been reduced (see Figure 1). This 3-D fluid motion, caused by pressure gradients, will be defined as *pressure gradient-induced flow.*

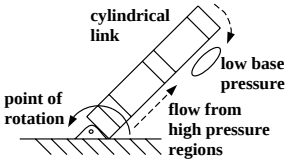

Figure 1: **Top view of representative pressure gradient-induced flow around rotating single link manipulator**

C. Current Work

As a continuation of the work in [7], this work focuses on hydrodynamic model development for a two-link arm, which is closer to a realistic underwater manipulator in that it has more configurability and possesses features found in multiple-link arms, such as elbow joints and end effectors at varying angles of incidence to the freestream. The desired uses for this model include accurate *a priori* analysis of system controller designs, precision manipulation from a free-swimming vehicle base, and the open loop planning of coordinated motions. These applications require a model that can accurately reflect the dynamics involved for various configurations and trajectories of the arm. The work presented here shows that the steady state loads on a planar 2 DOF underwater arm are insufficiently described by the constant coefficient models commonly used in the literature; joint torque predictions using constant coefficient models such as in Equation (1) were off by as much as 25% for simple slews with the elbow joint fixed at certain angles. Coefficients of existing models are not configuration-dependent; however, results show that there is a significant dependence of the hydrodynamic coefficient behavior on the configuration of the arm; therefore, a model that reflects this will be useful in determining trajectory planning solutions.

Flow visualization and preliminary analysis indicate that there are many flow regimes to consider for a full description of a 2 DOF arm, due to varying 3-D flow effects. This paper will focus on one type of motion for the arm, specifically, motion for which the elbow joint is fixed at an angle during shoulder joint slews, which can then be used in the development of a full model for a 2 DOF arm. A model for fixed elbow angle configurations will be developed by forming a modified extension to the single-link model in [7] based on flow visualization and joint torque measurements. The experimental system used in the research will be described. The approach and results of the model for various arm configurations will also be presented.

II. EXPERIMENTAL APPARATUS

The experimental work for this research was carried out on a planar 2 DOF manipulator built for use in the Stanford ARL test tank, a 2.3 m diameter, 1.5 m deep tank. Figure 2 shows the arm outside the tank. The manipulator and rig are suspended from an frame surrounding the tank. The manipulator has shoulder and elbow joints actuated by two variable reluctance motors. Each motor is a 1/4 hp motor with a 60:1 harmonic drive attached before the output shaft. Both motors are located at the shoulder joint; the second link is driven by a belt drive. Each link is made from hollow PVC pipe and is approximately 0.42 m long with a diameter of 0.05 m. The elbow joint was designed to blend in with the links as much as possible, so as not to dominate the flow characteristics, but also allow joint angles of ± 90 degrees. The shoulder can rotate a total of about 300 degrees, limited by the attached cables. Each motor has a capacitive encoder for position sensing of the output shafts. Torque sen-

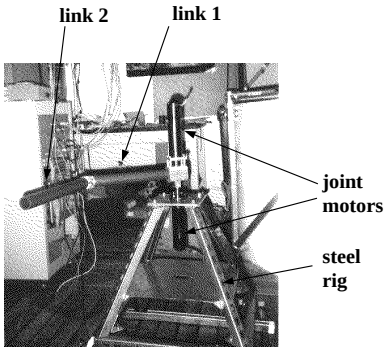

Figure 2: **Two-link manipulator, shown with one of its motors clamped onto a rig.**

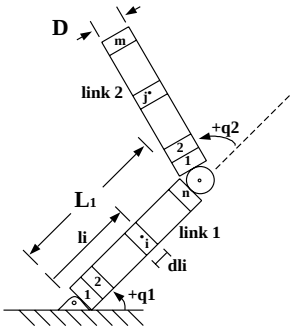

Figure 3: **Notation used for two-link manipulator.**

q_1 and q_2 are the joint angles, L_1 and L_2 are the link lengths, the diameter of both links is D, and l_k is the distance from the link's base joint to the centroid of the force on the k^{th} segment of a given link.

sors are mounted to measure the in-line torque at each joint. A PD control loop running at 230 Hz was able to achieve adequate position control for various commanded trajectories. Since the communications and control architecture are the same as for McLain's research work, the reader is referred to [7] for further system description.

III. HYDRODYNAMIC MODELING APPROACH

A. Flow Characteristics

There are many possible types of flow characteristics for two-link arm motion that can occur, depending on what flow regime the manipulator is operating in. This research has focused on the types of motion used when the manipulator is picking up or transferring specimens or tools— typically small acceleration slews over angular distances that are large enough that at least part of the manipulator has reached steady state. For these cases, the change in added mass parameters from those in [7] are negligible and drag is the dominant hydrodynamic effect to be modeled. The average Reynolds number for each link was assumed to be within the range $100 < Re < 10^5$. In this research, it was beneficial to use flow visualization to determine the important regions of the fluid flow to include in the model. A technique that has been used to analyze human swimming motion was modified for this purpose [1], using small sections of heat shrink linked together in a chain and attached along each link. This provides a nearly neutrally buoyant "stream" behind the trailing edge which indicates what the dominant flow characteristics are. A video camera mounted above the tank captures the dynamic images for post-analysis. See Figure 3 for a description of the notation used for referencing the 2 DOF manipulator and its motion.

For positive shoulder rotation, as indicated on Figure 3, the flow visualization for various joint trajectories will be described for cases where the elbow joint is held at a fixed angle. Figure 4 shows a snapshot of the experimental arm rotating in the tank with the elbow bent at +75 degrees. In addition, the observations of the

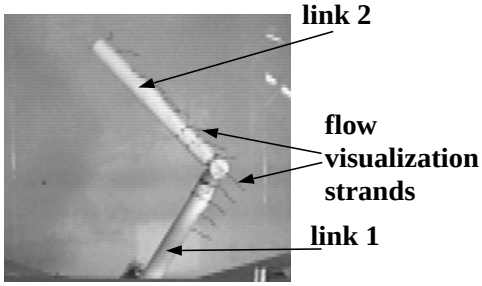

Figure 4: **Overhead flow visualization with elbow angle fixed at +75 degrees.**

The shoulder joint is rotating in a counter-clockwise direction. The strands of heat shrink strings can be seen on the trailing edge of the links.

flow behavior for various elbow angles are drawn in Figure 5. When q_2 is positive but still at small angles, as in Figure 5.1, the flow around the tip of the second link is increased, and there is still pressure gradient-induced flow from the first link onto the second one toward the tip of link 2. As q_2 increases, however, the fluid motion over the second link is in the direction of its freestream angle of attack, flowing from the tip of link 2 toward the elbow joint (see Figure 5.2). This type of fluid motion is defined as *geometric flow*. Consequently, the flow up the first link and down the second link meets slightly below the elbow at the top of link 1. For negative values of q_2, as shown in Figure 5.3, the geometric flow is in the same direction as the pressure gradient-induced flow towards the tip of the second link. There is no flow around the

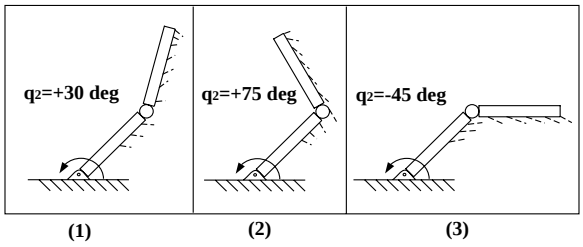

Figure 5: **Overhead flow description for different fixed elbow values.**

The dashed lines on the trailing edges of the links represent the flow visualization strings, as seen in Figure 4.

tip; instead, the flow bluffs off the end. When q_2 is close to -90 degrees, the flow up from the tip of the first link appears to *bounce off* the elbow and back down onto itself instead of continuing up the second link.

B. Model Formulation

For the given two-link arm, the joint torques due to drag using a constant coefficient model would be expressed as follows:

$$\tau_{shoulder} = \sum_{i=1}^{n} \frac{1}{2}\rho C_d V_{y,i} \mid V_{y,i} \mid D l_i dl_i +$$

$$\sum_{j=1}^{m} \frac{1}{2}\rho C_d V_{y,j} \mid V_{y,j} \mid D(l_j + L_1\cos(q_2))dl_j \quad (2)$$

$$\tau_{elbow} = \sum_{j=1}^{m} \frac{1}{2}\rho C_d V_{y_j} \mid V_{y_j} \mid D l_j dl_j \quad (3)$$

where τ is the indicated joint torque and C_d, ρ, V_y, and V_x are as described in Section I.

Based on the flow characteristics emphasized in the visualization of the two-link arm motion, a new model form was developed to reflect the important parameters in the hydrodynamics using the strip theory approach. The model for the joint torques due to drag can be represented by the following equations:

$$\tau_{shoulder} = \sum_{i=1}^{n} \frac{1}{2}\rho C_{d1}(s/D, q_2) V_{y,i} \mid V_{y,i} \mid D l_i dl_i +$$

$$\sum_{j=1}^{m} \frac{1}{2}\rho C_{d2}(s/D, q_2) V_{y,j} \mid V_{y,j} \mid D(l_j + L_1\cos(q_2))dl_j +$$

$$\frac{1}{2}\rho C_{d,end} V_{x,2} \mid V_{x,2} \mid \frac{\pi D^2}{4} L_1 \sin(q_2) \quad (4)$$

$$\tau_{elbow} = \sum_{j=1}^{m} \frac{1}{2}\rho C_{d2}(s/D, q_2) V_{y_j} \mid V_{y_j} \mid D l_j dl_j \quad (5)$$

This model differs from the constant coefficient one in three distinct ways: there are different pressure drag coefficients for links 1 and 2, these drag coefficients vary with both distance traveled and elbow angle, and a third drag term due to the end effector drag is added on to the shoulder torque equation. The model assumes that pressure drag forces are due to the perpendicular component of the linear velocity for each segment. The elbow torque is a function of the pressure drag on the second link. The first term in the shoulder torque equation is the component due to pressure drag on the first link. The second term is the component of the shoulder torque due to the pressure drag on the second link, and the third term is due to drag of the end effector. The model has three different drag coefficients, C_{d1} for the first link, C_{d2} for the second link, and $C_{d,end}$ for the end effector, since each section of the arm undergoes different pressure gradient and geometric flow effects. It is assumed that the transients of $C_{d1}(s/D)$ and $C_{d2}(s/D)$ will have the same form and time constant as in [7], but with different steady state values that will depend on the elbow angle and how each link is affected by the corresponding 3-D flow parallel to the links at that angle. Drag forces parallel to the link's longitudinal axis must also be taken into account due to the strong influence of the end effector orientation on the 3-D flow around the entire link. The elbow joint is not specifically modeled, but its effects on the fluid flow will be incorporated into C_{d1} and $C_{d,end}$.

One specific way the application of this new model differs from the use of a constant coefficient model is the dependency of the coefficients not only on elbow angle magnitude, which also affects other terms in both drag torque models, but also on the sign of the elbow angle, a characteristic that will affect solutions to trajectory planning algorithms.

To determine the values of the coefficients, curve fits to match the measured joint torques with those calculated by the complete dynamic model, including the hydrodynamics, were performed for a range of configurations for the fixed elbow cases. As described above, C_{d1} and C_{d2} are functions of distance traveled and elbow angle, while $C_{d,end}$ was assumed to remain constant.

IV. MODELING RESULTS

The results presented here are the fixed-elbow-angle parameter curve fits for the previously defined drag coefficients. The observed flow characteristics described above agree with the behavior of the coefficients in corresponding regimes. In general, wherever base pressure is relieved by 3-D flow on the links, the drag coefficient will tend to be decreased. Under conditions where the pressure is not relieved, or if flow is opposite the pressure gradient, the pressure drag forces, and consequently the drag coefficient, will be higher. See Figure 6 for a plot of the

fitted parameter curves for C_{d1} and C_{d2} for various elbow joint angles over the range of ±90 degrees, using constant acceleration/constant deceleration slews of the shoulder through 270 degrees of rotation. The results from three different curve-fits of slews are shown by the '+' symbols, with the solid line representing the average. The constant drag coefficient value of 1.1, used in [5], is represented by the dashed line. As indicated on the plots,

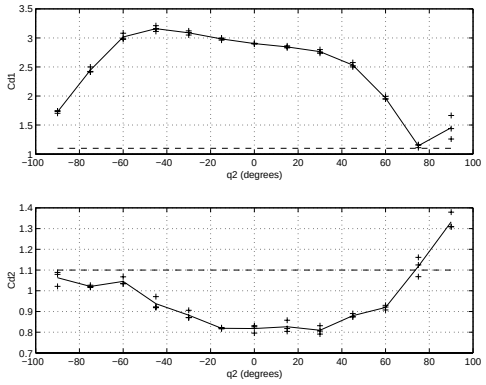

Figure 6: **Results from parameter fit for C_{d1}, C_{d2} for fixed elbow angle slews**

some general trends dominate the curve fits that can be supported by what was seen in the flow visualization. The first trend to note is how much the drag coefficient values for each link vary from what the previous constant coefficient models had suggested. C_{d1} can be up to two times greater for the new model than for the constant coefficient model, while C_{d2} varies between 18% greater and 28% lower than the constant coefficient value. For an elbow angle of 0 degrees, where the second link is positioned straight out, the drag coefficient of the first link ($C_{d1} = 2.9$) is actually much higher than that of the second link ($C_{d2} = .81$). This is due to the higher Reynold's numbers and lack of tip flow for the first link; the average drag coefficient for the entire arm in the "straight out" position matches that calculated by McLain's single-link model for the equivalent dimensions. For small angular values around 0 (±30 degrees), the flow up link 1 onto link 2 remains about the same, so C_{d1} doesn't vary much in this range. For small positive values, there is still both pressure gradient-induced flow up link 2, as well as flow around the tip, suggesting conditions for slightly lower values of C_{d2}. As q_2 increases in positive values, C_{d1} becomes lower, which can be compared to the flow around the elbow joint for these conditions, indicating that there is some pressure relief from link 2 onto link 1. Also for large positive angles, the geometric flow on the second link in the opposite direction becomes dominant, corresponding to the rise in C_{d2}.

For negative values of q_2, there is no flow around the tip, which would suggest an increase in the value of C_{d2} (as seen in the plot), but the rate of increase remains relatively small, most likely due to the presence of pressure gradient-induced flow that still occurs onto link 2 from link 1. At large negative values of q_2, where the flow appears to "bump" off of the second link and elbow back down onto the upper part of link 1, there is a decrease in its drag coefficient, C_{d1}, in this range. The constant value of $C_{d,end}$ was found to be 0.82 ±0.003.

This model for fixed elbow joint motion is consistent with the 3-D flow patterns seen around the elbow joint and tip and the behavior of the drag coefficients. Figures 7 through 9 show plots of the measured joint torques for various constant acceleration/deceleration slews compared with those predicted by this new model as well as the constant coefficient model. The new model, which allows for different coefficient behavior on both links, reduces the prediction errors by up to 2 times when compared to the torques predicted by the constant coefficient model for the slews shown, with error defined as the sum of the difference between measured and predicted torques throughout the slew, normalized by the sum of the measured torques .

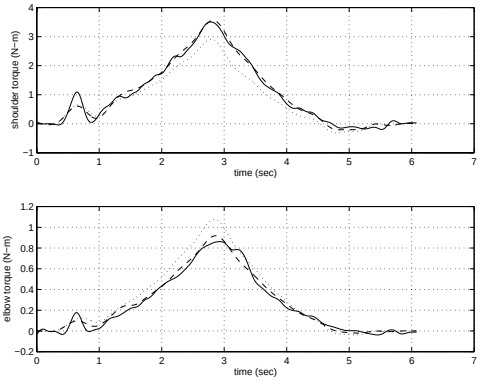

Figure 7: **Joint torques for an elbow angle of -75 degrees.**

The measured data is represented by the solid line, the torques predicted using the new model by the dashed line, and the torques predicted by the model used in [10] by the dotted line.

V. CONCLUSIONS

This paper presents research performed with the goal of improving the modeling technique for two-link robotic arms and extending the physical understanding of the flow past what is found in the literature. The new model, formulated for a two-link arm with a fixed elbow angle, includes separate drag coefficients for both links, each of which varies according to the flow conditions characterizing a given trajectory, plus a parallel drag term on the second link. Depending on the joint angles and trajecto-

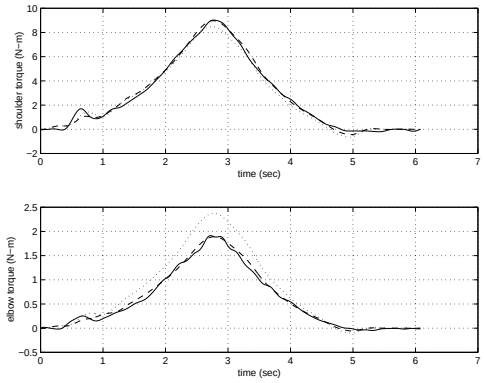

Figure 8: **Joint torques for an elbow angle of -90 degrees.**

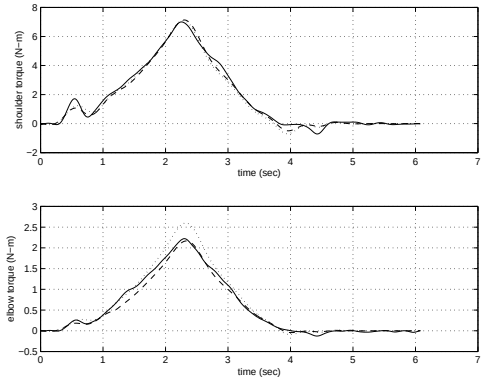

Figure 9: **Joint torques for an elbow angle of +60 degrees.**

ries, the flow can be dominated by various 3-D effects. Results have shown that using empirically-determined parameters in this form provides joint torque estimates that reduce modeling errors by twice those found when using a constant coefficient model for the typical trajectories considered. This representation can be used both in the modeling of an arm-vehicle system for preliminary analysis of control system designs, as well as control and planning algorithms for the arms themselves in order to achieve adequate endpoint placement.

E. Acknowledgments

This research is supported by the David and Lucile Packard Foundation under Grant #95-2777 with resources and support from MBARI.

REFERENCES

[1] HAY, J., AND THAYER, A. Flow Visualization of Competitive Swimming Techniques: the Tufts Method. *Journal of Biomechanics 22*, 1 (1989), 11–19.

[2] HOERNER, S. *Fluid-Dynamic Drag*. Sighard F. Hoerner, 1965.

[3] KATO, N., AND LANE, D. Co-ordinated control of multiple manipulators in underwater robots. In *Proceedings of the 1996 IEEE International Conference on Robotics and Automation* (Minneapolis, MN, April 1996), IEEE, pp. 2505–2510.

[4] KAWASHIMA, T., AND SHIMOGO, T. Positioning of floating underwater robot arm using counter arm and reaction wheel. In *Transactions of the Japan Society of Mechanical Engineers* (July 1994), JSME, pp. 2316–2322.

[5] LEVESQUE, B., AND RICHARD, M. Dynamic Analysis of a Manipulator in a Fluid Environment. *International Journal of Robotics Research 13*, 3 (1994), 221–231.

[6] MAHESH, H., YUH, J., AND LAKSHMI, R. A Coordinated Control of an Underwater Vehicle and Robotic Manipulator. *Journal of Robotic Systems 8*, 3 (June 1991), 338–370.

[7] MCLAIN, T., ROCK, S., AND LEE, M. Experiments in the Coordinated Control of an Underwater Arm/Vehicle System. *Journal of Autonomous Robots 3* (1996).

[8] RIGAUD, V., COSTE-MANIERE, E., ALDON, M., PROBERT, P., PERRIER, M., RIVES, P., SIMON, D., D. LAN AND, J. K., CASALS, A., AMAT, J., DAUCHEZ, P., AND CHANTLER, M. UNION: UNderwater Intelligent Operatino and Navigation. *IEEE Robotics and Automation* (March 1998), 25–35.

[9] SARPKAYA, T., AND ISAACSON, M. *Mechanics of Wave Forces on Offshore Structures*. Van Nostrand Reinhold Co., 1981.

[10] TARN, T., SHOULTS, G., AND YANG, S. Dynamic Model of an Underwater Vehicle With a Robotic Manipulator Using Kane's Method. *Autonomous Robots 3*, 2-3 (June-July 1996), 269–283.

[11] WANG, H. H., ROCK, S. M., AND LEE, M. J. OTTER: The design and development of an intelligent underwater robot. *Autonomous Robots 3*, 2-3 (June-July 1996), 297–320.